IOPscience iopscience.iop.org

Home Search Collections Journals About Contact us My IOPscience

Ni-silicide growth kinetics in Si and Si/SiO_2 core/shell nanowires

This article has been downloaded from IOPscience. Please scroll down to see the full text article.

2011 Nanotechnology 22 365305

(http://iopscience.iop.org/0957-4484/22/36/365305)

View the table of contents for this issue, or go to the journal homepage for more

Download details:
IP Address: 129.169.173.162
The article was downloaded on 07/02/2013 at 16:52

Please note that terms and conditions apply.

IOP PUBLISHING NANOTECHNOLOGY

Nanotechnology **22** (2011) 469601 (1pp) doi:10.1088/0957-4484/22/46/469601

Erratum

Ni-Silicide growth kinetics in Si and Si/SiO_2 core/shell nanowires

K Ogata, E Sutter, X Zhu and S Hofmann 2011
Nanotechnology **22** 365305

Received 27 September 2011
Published 27 October 2011

There is an error in the published article. In the first sentence of the last paragraph of section 4, the extrapolated diffusion coefficients were erroneously printed and should be:

$D_{\text{Ni_as-grown}} \sim 3.6 \times 10^{-12}$ cm^2 s^{-1} and
$D_{\text{Ni_oxidized}} \sim 9.6 \times 10^{-13}$ cm^2 s^{-1}.

 © 2011 IOP Publishing Ltd Printed in the UK & the USA

Nanotechnology **22** (2011) 365305 (7pp) doi:10.1088/0957-4484/22/36/365305

Ni-silicide growth kinetics in Si and Si/SiO_2 core/shell nanowires

K Ogata[1], E Sutter[2], X Zhu[1] and S Hofmann[1]

[1] Department of Engineering, University of Cambridge, 9 J J Thomson Avenue, Cambridge CB3 0FA, UK
[2] Center for Functional Nanomaterials, Brookhaven National Laboratory, Upton, NY 11973, USA

E-mail: sh315@cam.ac.uk

Received 1 June 2011, in final form 7 July 2011
Published 12 August 2011
Online at stacks.iop.org/Nano/22/365305

Abstract
A systematic study of the kinetics of axial Ni silicidation of as-grown and oxidized Si nanowires (SiNWs) with different crystallographic orientations and core diameters ranging from ∼10 to 100 nm is presented. For temperatures between 300 and 440 °C the length of the total axial silicide intrusion varies with the square root of time, which provides clear evidence that the rate limiting step is diffusion of Ni through the growing silicide phase(s). A retardation of Ni-silicide formation for oxidized SiNWs is found, indicative of a stress induced lowering of the diffusion coefficients. Extrapolated growth constants indicate that the Ni flux through the silicided NW is dominated by surface diffusion, which is consistent with an inverse square root dependence of the silicide length on the NW diameter as observed for ⟨111⟩ orientated SiNWs. *In situ* TEM silicidation experiments show that $NiSi_2$ is the first forming phase for as-grown and oxidized SiNWs. The silicide–SiNW interface is thereby atomically abrupt and typically planar. Ni-rich silicide phases subsequently nucleate close to the Ni reservoir, which for as-grown SiNWs can lead to a complete channel break-off for prolonged silicidation due to significant volume expansion and morphological changes.

S Online supplementary data available from stacks.iop.org/Nano/22/365305/mmedia

(Some figures in this article are in colour only in the electronic version)

1. Introduction

The self-organized bottom-up growth of semiconductor nanowires (NWs) offers the prospect of device engineering at the nanoscale for applications in nanoelectronics, photonics, energy generation/storage and sensors [1–3]. Reliable contact formation to individual NWs is crucial to these device applications, in particular regarding the typically small contact area. For Si, silicided contacts are widely used in the microelectronic industry; Ni silicides in particular can form at comparatively low temperatures and allow low resistivity phase formation for scaled device geometries [4]. Since Ni is the dominant diffusing species, for SiNWs an axial intrusion of Ni silicides occurs from patterned Ni contacts, which has the additional benefits of making the contact visible and of enabling a self-aligned gate length reduction for transistor fabrication [5–7]. Differences in the sequential phase formation behaviour between bulk and thin-film diffusion couples are well documented [4, 8], which highlights that for future integrated processing it is of key importance to understand the silicide formation kinetics for these nanoscale systems, particularly regarding size effects and the influence of stress and volume constraints.

For bulk and thin-film reactions the driving force for formation of a new phase can be, to first order, reduced to the difference in the enthalpies of formation between the product and the reactant phase, which for most Ni-silicide phases is large enough to make diffusion of the reactants through the growing phase the rate limiting factor [4]. For nanoscale systems, on the other hand, surface and interfacial energy terms become significant factors in the free energy of the system, and the effects are highlighted by recent literature on very thin films and NWs. Interfacial coherency at the Si/silicide growth front supports the observation of $NiSi_2$ as the first nucleated

 © 2011 IOP Publishing Ltd Printed in the UK & the USA

phase, in particular for ⟨111⟩ orientated SiNWs, followed by more metal-rich silicide phase segments in proximity to the Ni contacts [9, 10]. Further, the axial silicidation rate appears to increase with decreasing NW diameter, although there is considerable scatter among the limited literature [11–14]. Reported reaction rates are often difficult to compare and vary hugely, partly due to processing factors such as the quality of the NW interface to the Ni reservoir [15]. Hence the overall rate limiting factor and mechanism(s) remain unclear for these nanoscale systems.

Here we systematically compare the kinetics of Ni silicidation for as-grown and oxidized SiNWs with different crystallographic orientations and core diameters ranging from ∼10 to 100 nm. We show that for temperatures between 300 and 440 °C the length of the total axial silicide intrusion varies with the square root of time, and hence show that it is a diffusion limited process. A simple model allows us to extrapolate growth constants, which indicate that the Ni flux through the silicided NW is dominated by surface diffusion. Surface diffusion limited silicidation results in an inverse square root dependence of the silicide length on the NW diameter, which is consistent with our data for ⟨111⟩ orientated SiNWs. We find a clear retardation of the Ni-silicide formation for oxidized SiNWs, indicative of a stress induced lowering of the diffusion coefficients. Our *in situ* TEM silicidation experiments show that $NiSi_2$ is the first forming phase for as-grown and oxidized SiNWs of ⟨111⟩ orientation as well as, for instance, ⟨110⟩ orientation. The silicide–SiNW interface is thereby atomically abrupt and typically planar. We observe that Ni-rich silicide phases subsequently nucleate close to the Ni contact, which for as-grown SiNWs can lead to a complete channel break-off for prolonged silicidation due to significant volume expansion and morphological changes.

2. Experimental details

The SiNWs were synthesized by catalytic chemical vapour deposition (CVD) using silane as precursor and Au as the catalyst. Au (∼2 nm, measured by a quartz crystal balance) was evaporated onto thermally oxidized Si(100) wafers (200 nm SiO_2), onto perforated Si nitride transmission electron microscopy (TEM) membranes (Agar Scientific) and, for epitaxial growth, onto HF-dipped Si(111) wafers. The samples were transferred to a cold-wall CVD system with a 10^{-8} mbar base pressure, where they were heated in H_2 and then exposed to H_2 diluted SiH_4 for 10 min. For growth on amorphous Si oxide or nitride support, a H_2/SiH_4 ratio of 170/30 sccm at 15 mbar total pressure at 400 °C was used, resulting in SiNWs of average diameter ∼40 nm and length >5 μm with a distribution of growth directions and a ∼2 nm native oxide after air exposure. For epitaxial growth, the Au was e-beam patterned on the Si(111) support and a H_2/SiH_4 ratio of 190/8 sccm at 6 mbar total pressure and 500 °C was used, resulting in a predominant ⟨111⟩ NW growth direction. For the epitaxial growth recipe, Au was found to decorate the SiNW side walls and hence an additional wet etching step (NH_4F:HF = 7:1) was introduced to remove most of the Au. SiNW oxidation was carried out in a hot-wall furnace (base pressure 10^{-4} mbar) at 900 ° C in 960 mbar O_2. Oxidation for ∼10 min resulted in a SiO_x shell thickness ranging from 10 to 20 nm.

In order to investigate the Ni/Si solid state reaction, SiNWs were transferred onto pristine SiO_2 (200 nm)/Si substrates and Ni contact structures (5 × 5 μm^2, with a pitch of 15 μm) were patterned by e-beam lithography using polymethyl methacrylate (PMMA) resist. Prior to Ni evaporation (∼60 nm), the samples were treated with HF for 10 and 30 s for non-oxidized/oxidized NWs, respectively. The under-etched length for oxidized NWs was thereby kept within tens of nanometres. TEM compatible samples were fabricated based on the same procedure but using SiNWs grown directly onto perforated Si nitride TEM membranes. Regarding the samples for *ex situ* Ni-silicide observation, silicidation was initiated in an Ar atmosphere at ∼2 × 10^{-4} mbar at temperatures ranging from 300 to 440 °C for 2–35 min in the cold-wall CVD reactor. All quoted temperatures refer to pyrometer measurements (IMPAC IGA 8 Plus, single band 1.6 μm) using a carbon nanotube forest covered reference sample for which we assume an emissivity of 1. The temperature for a run thereby refers to the maximum of the time-dependent annealing profile. The samples were characterized mainly by scanning electron microscopy (SEM; Hitachi S-5500) and TEM (FEI, Tecnai G220 and Titan 80–300; JEOL JEM-3010). For selected TEM compatible samples, the silicidation was carried out *in situ* during TEM observation with a heating holder operated in a vacuum.

3. Results

Figure 1 compares representative SEM and TEM images of as-grown and oxidized SiNWs after Ni silicidation. We cannot detect any axial silicidation for temperatures below ∼280 °C for annealing times up to 7 h, i.e. we cannot reproduce a previous report on significant SiNW Ni silicidation rates at 280 °C [11]. Our TEM analysis (figures 1(b), (d)) indicates that the Ni intrusion leads to formation of $NiSi_2$ at the interface with the SiNW. This is in agreement with previous literature [5, 9, 16], albeit we find the $NiSi_2$ phase not only for ⟨111⟩ oriented NWs but also, for example, at the interface to ⟨110⟩ NWs. The $NiSi_2$ is typically single crystalline and its Si interface is atomically abrupt and can be, but not necessarily always is, a straight plane. In figures 1(b)–(d) we identify the commonly found epitaxial relations of $NiSi_2$(111) ∥ Si(111); $NiSi_2$[110] ∥ Si[110] for both as-grown/oxidized SiNWs, respectively.

We define the total length of the axial Ni-silicide intrusion starting from the Ni pad as $L_{Ni_xSi_y}$ (figures 1(a) and (c)). Figure 2 shows $L_{Ni_xSi_y}$ plotted over annealing time for as-grown NWs (with a native oxide layer) and for thermally oxidized NWs. The annealing time is thereby defined as the time for which the measured annealing profile is above 350 °C (figure 2 inset), which is the temperature above which the reaction occurs at an observable rate at the given conditions. Two sets of data are compared for each NW type: (1) an average of typically ∼15 NWs for a single annealing step and (2) data for an individual NW for sequential annealing, as

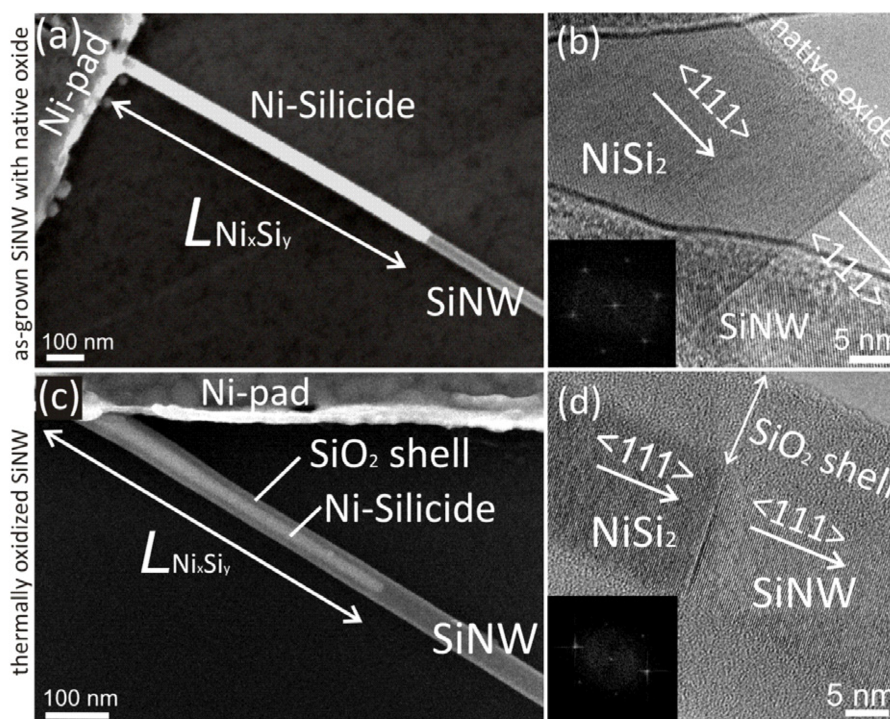

Figure 1. ((a), (c)) SEM and ((b), (d)) TEM images of as-grown ((a), (b)) and oxidized ((c), (d)) SiNWs Ni-silicided at ∼440 °C (SEM) and ∼550 °C (TEM) for 6 min, respectively. The insets in (b) and (d) show the FFT of the respective silicide regions close to the Si.

shown by the respective SEM image series. Figure 2 clearly shows that (1) and (2) give comparable results within the experimental error. $L_{Ni_xSi_y}$ follows a square root dependence with annealing time, whereby $L_{Ni_xSi_y}$ is significantly shorter for oxidized NWs at any given time >5 min. We note that the SiNWs are solidly covered by the Ni pads even after more than 40 min annealing, which shows that the reaction is not limited by the Ni reservoir. We confirm the same parabolic trend with a 100 nm thick Ni pad. We further note that selected as-grown SiNWs that were additionally treated with HF for a second time after the Ni evaporation show no measurable difference from single HF treated samples. Our data provide clear evidence for a diffusion limited regime, whereby the retardation for oxidized SiNWs is due to a stress reduced Ni flux.

Figure 3 shows that prolonged Ni silicidation for as-grown SiNWs leads to an increased likelihood of a complete Si channel break-off. This reflects the formation of Ni-rich silicide phases close to the Ni contact. Defining a modified Pilling–Bedworth ratio R_{PB} as the ratio of the density of Si atoms in Si to the density of Si atoms for the silicide phase [17], we note that whereas R_{PB} is basically 1 for $NiSi_2$, it increases steadily the more Ni-rich the silicide phase becomes. This can cause significant morphological changes of the silicided NW close to the Ni pad and, ultimately, break-off. We did not observe such break-off behaviour for oxidized SiNWs under the given conditions. This indicates that the oxide shell restricts radial volume expansion, hence such significant morphological changes.

Figure 4(a) shows the measured variation of $L_{Ni_xSi_y}$ versus SiNW core diameter for two different annealing times at ∼440 °C. The plot includes data for as-grown as well as oxidized SiNWs and we emphasize that the data reflect SiNWs with a range of different crystallographic orientations. Figure 4(a) shows no clear variation of the silicidation rate with SiNW diameter. In order to eliminate the possible orientation dependence of the Ni silicidation, we carried out a series of silicidation experiments with epitaxially seeded, hence predominantly ⟨111⟩ orientated, SiNWs. As shown in figure 4(b), $L_{Ni_xSi_y}$ for these ⟨111⟩ orientated SiNWs increases for decreasing NW diameter, which can be fitted by an inverse square root dependence. We note that our data are consistent with data for SOI-based top-down fabricated SiNWs [12, 14].

In order to investigate the reaction mechanisms in more detail, we carried out the silicidation process *in situ* during lattice- and time-resolved TEM observation. We emphasize that here we transferred our process to TEM compatible membranes unlike previous reports on *in situ* TEM silicidation which relied on difficult-to-control point contact reactions and, interestingly, for which the Ni silicidation started away from the actual Ni contact [18]. In fact, the rate limiting factor for these previous *in situ* studies was argued to be the Ni diffusion flux through the SiNW to the actual silicide–Si interface [18], which is significantly different from the process we study here. Figure 5 shows an *in situ* high resolution TEM image sequence of the propagating $NiSi_2$–SiNW interface at 360 °C. The interface has an epitaxial relationship of $NiSi_2(111) \parallel Si(111)$; $NiSi_2[110] \parallel Si[110]$ where a dark contrast region appears to precede the main $NiSi_2$/Si interface (figure 5). Due to the projected nature of the TEM imaging we cannot unambiguously assign this contrast

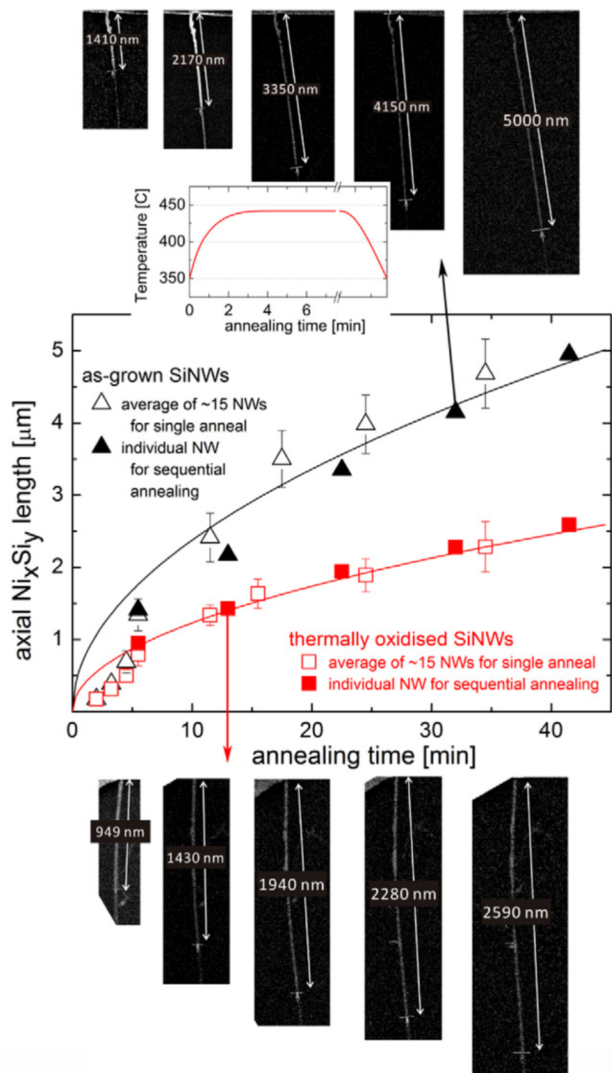

Figure 2. Total Ni_xSi_y length $L_{Ni_xSi_y}$ versus time for as-grown and oxidized SiNWs at ∼440 °C. The fitted lines represent a square root dependence. Open symbols refer to data points averaged for about 15 different NWs for a single annealing step. The error bar represents the standard error. Filled symbols refer to an individual NW annealed sequentially as shown by the respective SEM image series at the top (as-grown NW) and bottom (oxidized NW). The annealing time is defined via the measured temperature profile (inset) as time above 350 °C.

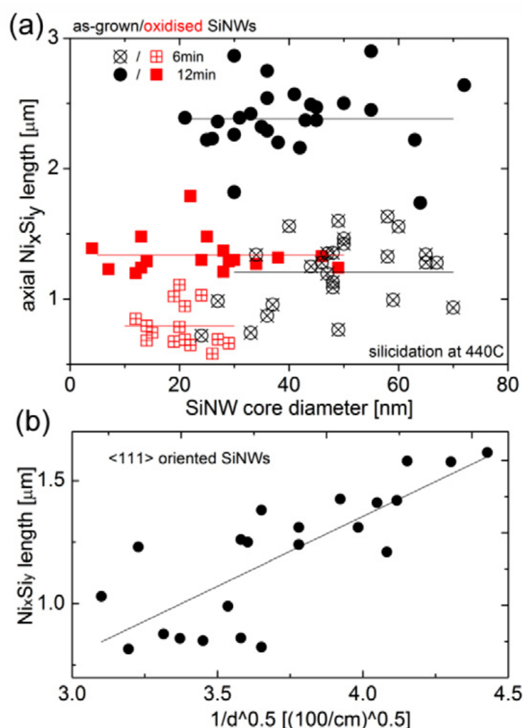

Figure 4. (a) $L_{Ni_xSi_y}$ versus SiNW core diameter for two different annealing times of 6 min and 12 min at ∼440 °C. The plot includes data for as-grown and oxidized SiNWs and reflects SiNWs with a range of different crystallographic orientations. The horizontal (solid) lines highlight the average $L_{Ni_xSi_y}$ for each set of plots. (b) Silicidation rate versus diameter for ⟨111⟩ orientated SiNWs. The fitted line represents an inverse square root dependence.

but one could speculate about a stepped interface or a very high interstitial Ni concentration close to the interface. We can exclude wedge-shaped silicide protrusions or a significantly increased advancement of Ni exclusively at the SiNW surface at any stage of the process. This is in contrast to model calculations by Katsman *et al* [13]. For prolonged annealing we can clearly identify the formation of more Ni-rich silicides close to the Ni pads, in agreement with a recent TEM study [9]. We can typically assign a Ni_3Si phase towards the Ni pads, both for as-grown and oxidized SiNWs. Based on bulk data [4], Ni_3Si has a R_{PB} of more than 2, but interestingly for oxidized

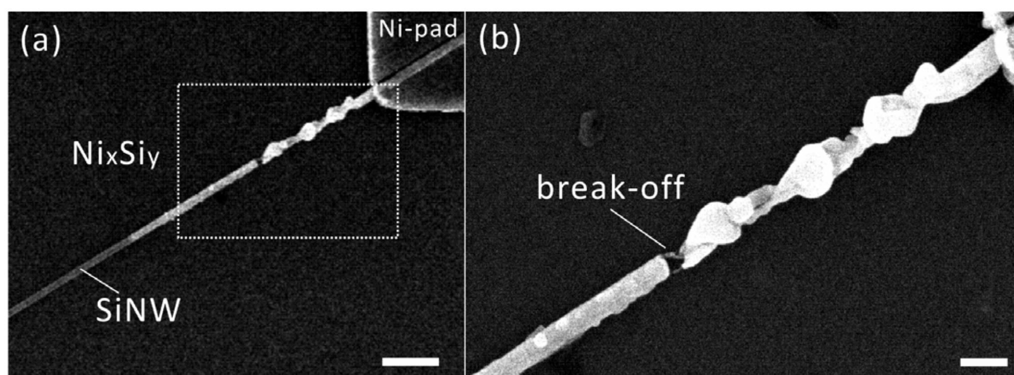

Figure 3. SEM images of as-grown SiNWs after 12 min of Ni silicidation at ∼440 °C. Part (b) is a magnified image of the area highlighted in (a), the scale bars in (a) and (b) are 300 and 100 nm, respectively.

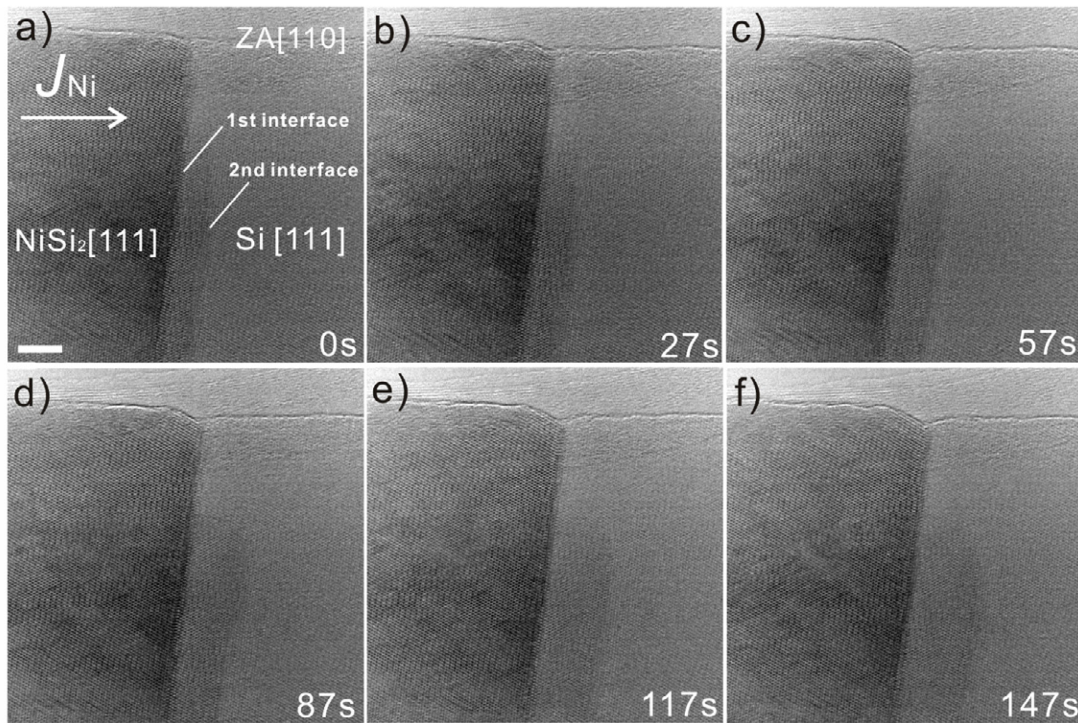

Figure 5. *In situ* TEM image sequence of a propagating $NiSi_2$–SiNW interface at 360 °C (corresponding to supplementary data video S1 stacks.iop.org/Nano/22/365305/mmedia). The scale bar is 5 nm.

SiNWs we find no matching significant radial expansion. The TEM data reported in the literature show significant radial expansion for metal-rich silicides, in particular at the lengthy HF undercut areas of oxidized SiNWs [9]. Here we tried to minimize this undercut. We find, however, that the SiO_2 layer sometimes starts to be consumed by the silicidation process. We also cannot identify clear, sharp interfaces between the silicide phases.

4. Discussion

We rationalize the NW silicidation by a simple model as outlined in figure 6. With Ni as the dominating diffusing species, we assume three key fluxes: (1) flux of Ni through the interface between contact pad/Ni reservoir and the NW, (2) Ni diffusion flux along the silicide phase(s) of the NW, and (3) a silicidation reaction at the Ni_xSi_y/SiNW interface. These three fluxes can be expressed as:

$$F_1 = k_1 \frac{(C_{\mathrm{res}} - C_0)}{d_{\mathrm{r}}} \tag{1}$$

$$F_2 = k_2 \frac{(C_0 - C_{\mathrm{I}})}{L_{\mathrm{Ni}_x\mathrm{Si}_y}} \tag{2}$$

$$F_3 = k_3 C_I \tag{3}$$

where k_x are the respective transport/reaction constants, C_{res}, C_0 and C_{I} are the nickel concentrations in the reservoir, at the Ni/Ni_xSi_y and Ni_xSi_y/SiNW interfaces and d_{r} is the thickness of the interfacial layer between the Ni pad and NW. Under steady state conditions $F_1 = F_2 = F_3 = F$, and the silicidation rate is given by

$$\frac{\mathrm{d}L_{\mathrm{Ni}_x\mathrm{Si}_y}}{\mathrm{d}t} = \frac{F}{N_{\mathrm{Ni}}} \tag{4}$$

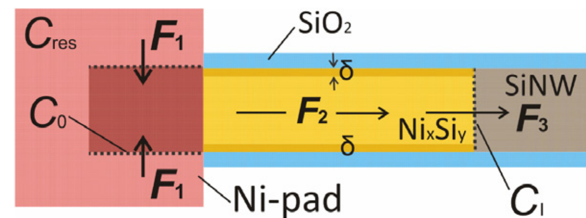

Figure 6. Schematic of the Ni-silicide intrusion process. F_1 is the Ni flux from the reservoir to the NW. F_2 constitutes the Ni diffusion through the silicide(s), whereby δ indicates a surface/interface layer of high diffusivity. F_3 represents the interfacial reaction rate at the silicide/Si interface.

where N_{Ni} is the number of nickel atoms incorporated per unit volume of silicide grown. The model can be extended to the sequential formation of multiple silicide phases, but here we restrict ourselves to a simplistic model to highlight the key rate limiting factor. A consideration of $F_1 = F_2$, neglecting F_3, has been reported by Yaish *et al* [15]. This shows two rate limiting scenarios: a square root variation of $L_{\mathrm{Ni}_x\mathrm{Si}_y}$ versus annealing time results if F_2 is rate limiting, whereas a poor quality interface can give a linear growth regime over an initial or even the whole period. A consideration of $F_2 = F_3$ reflects a Deal–Grove like model, where the system is initially reaction

limited with a linear term dominating, i.e. $L_{\mathrm{Ni}_x\mathrm{Si}_y} \sim t$, but for longer $L_{\mathrm{Ni}_x\mathrm{Si}_y}$ a parabolic term dominates: $L_{\mathrm{Ni}_x\mathrm{Si}_y} \sim \sqrt{t}$.

As shown in figure 2 our data can be fitted reasonably well with a square root of time dependence, which provides clear evidence for diffusion limited growth, i.e. F_2 is rate limiting. As for annealing times of 5 min or less the heating ramp comprises a significant part of the reaction time, and we cannot comment in detail on a potentially initial linear behaviour. A challenge well known in the silicide literature is the interpretation of k_2. In general, a diffusion flux is driven by a gradient in the chemical potential and the chemical potential is proportional to the concentration gradient only for dilute systems or ideal solid solutions. Further, concentration gradients are typically unknown. Hence a better representation of F_2 for silicide growth is:

$$F_2 = C_{\mathrm{Ni}} M_{\mathrm{Ni}} \left(-\frac{\partial \mu_{\mathrm{Ni}}}{\partial L}\right) = C_{\mathrm{Ni}} \left(\frac{D_{\mathrm{Ni}}}{kT}\right) \left(\frac{\Delta G}{L_{\mathrm{Ni}_x\mathrm{Si}_y}}\right) \quad (5)$$

where M_{Ni} denotes the Ni mobility, which relates to the tracer diffusion coefficient D_{Ni} via the Nernst–Einstein equation $D_{\mathrm{Ni}} = M_{\mathrm{Ni}} kT$, with k denoting the Boltzmann constant [19]. C_{Ni} is the concentration and $\frac{\partial \mu_{\mathrm{Ni}}}{\partial L}$ is the gradient of the chemical potential along the NW channel. For simplicity the latter is taken as $\frac{\Delta G}{L_{\mathrm{Ni}_x\mathrm{Si}_y}}$, where ΔG is the free energy change per moving Ni atom [8, 19]. We define the growth constant $\kappa = (\frac{2\Delta G D_{\mathrm{Ni}}}{kT})$, hence $L_{\mathrm{Ni}_x\mathrm{Si}_y} = \sqrt{\kappa t}$. Fitting in figure 2 gives a value of $\kappa_{\text{as-grown}} \sim 9 \times 10^{-11}$ cm^2 s^{-1} and $\kappa_{\text{oxidized}} \sim 2 \times 10^{-11}$ cm^2 s^{-1}, respectively. The extrapolated values compare well to tabulated values for κ measured for thin-film and bulk-silicide formation [8], which at 440 °C range between 10^{-13} and 10^{-11} cm^2 s^{-1} depending on phase and conditions. Moreover, our data show that κ for oxidized SiNWs is lower, indicating a decrease of the growth constant due to internal stress.

We can extrapolate $D_{\text{Ni_as-grown}} \sim 3.6 \times 10^{-12}$ cm^2 s^{-1} and $D_{\text{Ni_oxidized}} \sim 9.6 \times 10^{-12}$ cm^2 s^{-1}, assuming a single Ni-silicide phase ($NiSi_2$, $\Delta G_{\mathrm{NiSi}_2} = -77.5$ kJ mol^{-1}) [4]. Tabulated values for bulk tracer diffusion coefficients D_{Ni} in a Ni_2Si or Ni_5Si_2 matrix at the given temperature range between 10^{-17} and 5×10^{-14} cm^2 s^{-1} [8], hence appear too small to be consistent with our data. This indicates that a surface/interface contribution needs to be considered. Models describing grain boundary diffusion commonly assume a layer of thickness δ with a much higher diffusivity than in the bulk, and for Type-A kinetics an effective diffusivity is given by [8]

$$D_{\mathrm{Ni-eff}} = (1-g)D_{\mathrm{B}} + g D_{\mathrm{S}} \quad (6)$$

where D_{B}, D_{S} denote bulk and surface diffusion terms, respectively, and $g = \frac{p\delta}{d_{\mathrm{NW}}}$ with d_{NW} denoting the NW diameter and p a shape-dependent numerical factor. Tabulated values for grain boundary diffusion coefficients D_{S} in a Ni_2Si or Ni_5Si_2 matrix at the given temperature are in a range between 10^{-11} and 5×10^{-9} cm^2 s^{-1} [8], hence with $g = 0.01$ agree reasonably well with our extrapolated D_{Ni} values. However, we note that the nature of a grain boundary for a bulk sample can be quite different from the surface of our silicided NWs, hence the validity of the comparison to limited, tabulated data is restricted. We note that if F_2 is entirely dominated by fast diffusion in a surface layer of the silicided NW, then $L_{\mathrm{Ni}_x\mathrm{Si}_y} \sim 1/\sqrt{d_{\mathrm{NW}}}$ for a given annealing time and temperature. This is consistent with figure 4(b).

5. Conclusions

We study the axial Ni silicidation for as-grown and oxidized SiNWs with different crystallographic orientations and core diameters ranging from ~10 to 100 nm. Our data provide clear evidence that the rate limiting step is Ni diffusion through the growing silicide phase(s), whereby the retardation observed for oxidized SiNWs is due to a stress reduced Ni flux. We extrapolate growth constants via a simple model, which allows us to argue that this Ni flux through the silicided NW is dominated by surface diffusion and to rationalize an inverse square root dependence of the silicide length on the NW diameter. Our *in situ* TEM silicidation experiments show that $NiSi_2$ is the first forming phase for as-grown and oxidized SiNWs of various crystallographic orientations, whereby the silicide–SiNW interface is atomically abrupt and typically planar. We observe that Ni-rich silicide phases subsequently nucleate close to the Ni pad, which for as-grown SiNWs can lead to a complete channel break-off for prolonged silicidation due to significant volume expansion and morphological changes.

Acknowledgments

The authors acknowledge T Iijima, Y Hayashi (Department of Frontier Materials, Nagoya Institute of Technology) for help regarding the oxide thickness calibration. KO acknowledges funding from the Japanese Ministry of Education, Culture, Sports, Science and Technology (MEXT) and SH funding from the Royal Society. Part of this work performed at the Center for Functional Nanomaterials, Brookhaven National Laboratory, which is supported by the US Department of Energy under contract no. DE-AC02-98CH10886.

References

[1] Appenzeller J, Knoch J, Bjork M I, Riel H, Schmid H and Riess W 2008 *IEEE Trans. Electron Devices* **55** 2827
[2] Chan C K, Peng H L, Liu G, McIlwrath K, Zhang X F, Huggins R A and Cui Y 2008 *Nature Nanotechnol.* **3** 31
[3] Boettcher S W, Spurgeon J M, Putnam M C, Warren E L, Turner-Evans D B, Kelzenberg M D, Maiolo J R, Atwater H A and Lewis N S 2010 *Science* **327** 185
[4] Chen L J 2004 *Silicide Technology for Integrated Circuits* (London: Institute of Engineering and Technology)
[5] Weber W M *et al* 2006 *Nano Lett.* **6** 2660
[6] Chou Y C, Wu W W, Chen L J and Tu K N 2009 *Nano Lett.* **9** 2337
[7] Schmitt A L, Higgins J M, Szczech J R and Jin S 2010 *J. Mater. Chem.* **20** 223
[8] Landolt-Bornstein (ed) 1998 *Diffusion in Semiconductors* vol III/33 (Berlin: Springer)
[9] Lin Y C, Chen Y, Xu D and Huang Y 2010 *Nano Lett.* **10** 4721
[10] Dellas N S, Liu B Z, Eichfeld S M, Eichfeld C M, Mayer T S and Mohney S E 2009 *J. Appl. Phys.* **105** 094309
[11] Appenzeller J, Knoch J, Tutuc E, Reuter M and Guha S 2006 *IEDM Tech. Dig.* **1** 302

[12] Habicht S, Zhao Q T, Feste S F, Knoll L, Trellenkamp S, Ghyselen B and Mantl S 2010 *Nanotechnology* **21** 105701
[13] Katsman A, Yaish Y, Rabkin E and Beregovsky M 2010 *J. Electron. Mater.* **39** 365
[14] Kamimura H and Iwai H 2009 *Thesis* Tokyko Institute of Technology
[15] Yaish Y E, Katsman A, Cohen G M and Beregovsky M 2011 *J. Appl. Phys.* **109** 094303
[16] Weber W M, Geelhaar L, Unger E, Cheze C, Kreupl F, Riechert H and Lugli P 2007 *Phys. Status Solidi* b **244** 4170
[17] Walter J L, Jackson M R and Sims C T 1988 *Alloying* (Metals Park, OH: ASM International)
[18] Lu K C, Tu K N, Wu W W, Chen L J, Yoo B Y and Myung N V 2007 *Appl. Phys. Lett.* **90** 253111
[19] d'Heurle F M and Gas P 1985 *J. Mater. Res.* **1** 205